Available online at www.sciencedirect.com
SCIENCE DIRECT®
Chemical Engineering and Processing 44 (2005) 363–374
Chemical Engineering and Processing
www.elsevier.com/locate/cep

Hydrodynamics and mass transfer in an upflow monolith loop reactor

C.O. Vandu, J. Ellenberger, R. Krishna*

Department of Chemical Engineering, University of Amsterdam, Nieuwe Achtergracht 166, 1018 WV Amsterdam, The Netherlands

Received 19 February 2004; received in revised form 27 May 2004; accepted 27 May 2004
Available online 23 August 2004

Abstract

The hydrodynamics and mass transfer characteristics of a monolith loop reactor, with upflow of gas and liquid phases through the channels, have been investigated and compared with conventional internal airlift reactor and bubble column configurations. The volumetric mass transfer coefficient, $k_L a$, is higher for monolith reactors than for airlift and bubble columns. This improvement is due to the superior mass transfer characteristics of Taylor flow in narrow capillaries. In order to gain further insight into the mass transfer from Taylor bubbles, experimental results are presented on the unit cell lengths and the Taylor bubble rise velocity.

Keywords: Monolith reactors; Gas holdup; Taylor bubbles; Bubble columns; Internal airlift; Mass transfer coefficient

1. Introduction

Monolith loop reactors are gaining considerable attention from academia and industry alike for carrying out solid catalysed gas–liquid reactions [1–4]. Monolith loop reactors are being applied in the laboratory studies and in commercial practice for carrying out reactions such as hydrogenations [5–7], hydrodesulphurization [8], oxidations [9], bioremediation [10] and Fischer–Tropsch synthesis [11,12]. Monolith reactors offer many potential advantages over trickle beds, slurry bubble columns and airlifts that include low pressure drop, high mass transfer rates, and ease of scale up [5,13,14]. Stankiewicz [14] provides an example of a process for which an in-line monolith reactor is 100 times smaller in size than a conventional reactor and therefore represents a truly intensified process. Most of the published experimental studies relate to downflow of both gas and liquid phases in monoliths [7,13,15–19] and very little information is available on upflow operation of gas and liquid [2]. In both upflow and downflow operations of monolith reactors we need to have uniform distribution of gas and liquid phases through the various channels.

The first major objective of the present work is to study the hydrodynamics and mass transfer in an upflow monolith loop reactor. The second objective is to develop the corresponding data on gas holdup, ε_G, and volumetric mass transfer coefficient, $k_L a$, also for a bubble column and airlift, using the same column geometry and gas distribution device. In the study upflow monolith loop reactors of two different heights were employed. The data generated in this work would be helpful in choosing the right reactor type for any given process.

2. Experimental setups

2.1. Monolith loop reactor

Experiments were performed in two upflow monolith loop reactor column configurations, schematically represented in Fig. 1. The setup shown on the left in Fig. 1 has a taller monolith bundle section (of height 2.1 m) than the setup shown in the inset, which has a monolith riser of height 0.65 m. For convenience, these setups would be referred to as tall and short monolith reactors, respectively. Hydrodynamic and mass transfer studies were carried out in both setups. The idea of the short monolith reactor came into being due to the possibility of saturation of the upflowing liquid phase (water) in the tall monolith reactor during mass transfer experiments (a detailed discussion on this is presented later). Each reactor comprised of an outer column, a riser column and a gas–liquid separation unit. The outer column and gas–liquid separator were constructed of polyacrylate

* Corresponding author. Fax: +31-20-525-5604.
E-mail address: r.krishna@uva.nl (R. Krishna).

0255-2701/$ – see front matter © 2004 Elsevier B.V. All rights reserved.
doi:10.1016/j.cep.2004.05.011

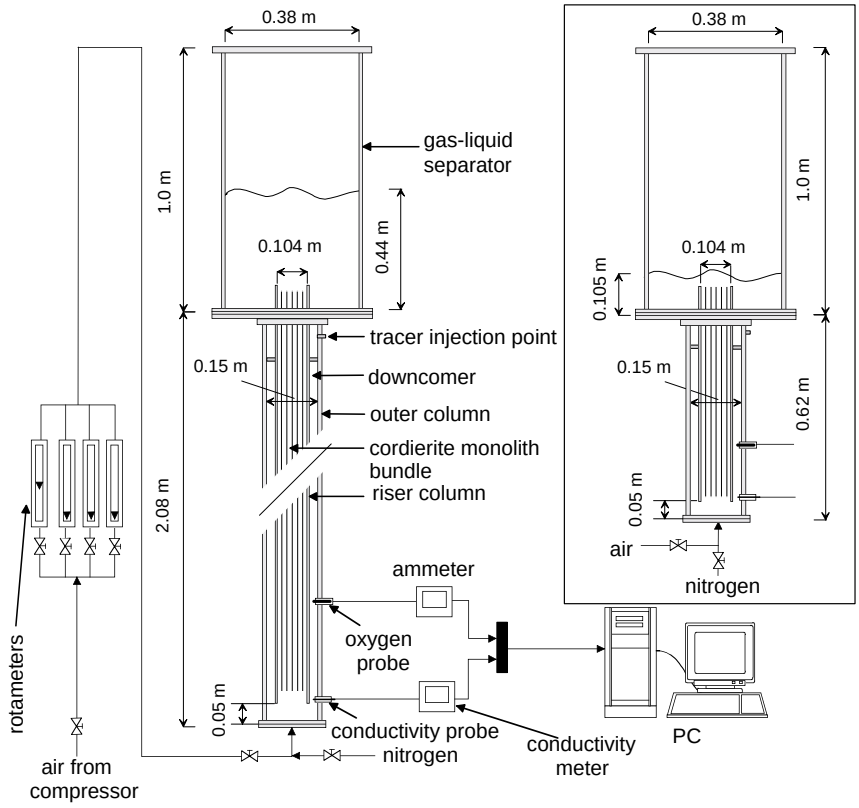

Fig. 1. Experimental setup for the tall and short monolith loop reactors (the details of the latter are shown in the inset to the figure). Further details of the setup, including photographs and video recordings of the hydrodynamics are available elsewhere [20].

with the riser column fabricated from glass. The riser column was concentrically positioned in the outer column, with a clearance of 0.05 m. The annular space between the riser and outer columns formed the downcomer section of the reactor. The riser column, outer column and gas–liquid separator had internal diameters of 0.104, 0.15 and 0.38 m, respectively.

A monolith bundle consisting of symmetrically aligned cordierite monolith pieces (Corning GmbH, Germany) each with 48 cells per square inch (cpsi) was inserted in the riser tube of each reactor. Each monolith had square-shaped channels with sides of approximately 3.01 mm and an estimated void fraction of 67%. In the tall reactor, the monolith bundle consisted of seven monolith pieces with a combined height of 2.05 m. The monolith bundle in the short reactor comprised of two monolith pieces with a combined height of 0.6 m. Fig. 2 shows a schematic representation of the monolith cross-section.

Both monolith reactors had a 0.1 m-diameter, 1 mm-thick brass plate gas distributor with perforated holes of 0.5 mm diameter on a triangular pitch of 7 mm. Gas flow was regulated by the use of pre-calibrated rotameters (Sho-Rate Brooks Instruments BV, The Netherlands) aligned in parallel or by a manually operated control valve.

Further details of the monolith setups, including photographs and video recordings of the hydrodynamics are available elsewhere [20].

2.2. Airlift loop reactor and bubble column reactor

Corresponding experimental studies were also carried out in an internal airlift loop reactor and a bubble column. The setup of the airlift loop reactor was a modification of the tall monolith loop reactor in which the glass riser column

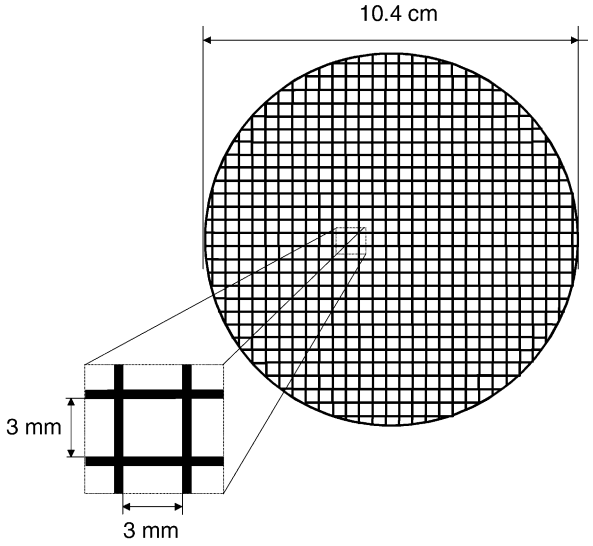

Fig. 2. Schematic representation of the 48 cpsi square-channel cordierite monolith used in this study.

Table 1
Dimensions of the reactor configurations employed

	Height of riser column (m)	Inner diameter of riser column (m)	Outer diameter of riser column (m)	Inner diameter of outer column (m)	Height of monolith segments (m)
Tall monolith loop: square channel	2.1	0.104	0.111	0.15	2.05
Short monolith loop: square channel	0.65	0.104	0.111	0.15	0.6
Airlift lift loop reactor	2.1	0.1	0.11	0.15	–
Bubble column reactor	–	–	–	0.15	–

of the latter and its monolith bundle were replaced by a 0.1 m-diameter polyacrylate riser tube. Thus, like the monolith loop reactor, the airlift loop reactor comprised of an outer column, a riser column and a gas–liquid separation unit. The same gas distributor was employed in both the monolith and airlift loop reactor configurations. Further details of the airlift setup, including photographs and video recordings of the hydrodynamics are available elsewhere [21].

The bubble column, with an internal diameter of 0.15 m and a height of 4 m was made of polyacrylate. It however had a 0.15 m-diameter, 1 mm-thick brass plate gas distributor with perforated holes 5 mm in diameter on a 7 mm pitch. Pressure taps, used in the determination of gas holdup, were installed along the height of the bubble column. Two of these taps were connected to pressure ports on a Validyne DP15 pressure transducer, which was in turn coupled to a PC via an analogue to digital converter system consisting of the pressure transducer, a voltmeter and an analogue-to-digital (AD) converter card on the PC. Further details of the bubble column setup, including photographs and video recordings of the hydrodynamics are available elsewhere [22].

Table 1 gives a summary of the principal dimensions of the four reactors employed in this study.

2.3. Single capillary experiments

Experiments were also performed in an upflow single capillary setup, described in detail elsewhere [23]. This setup consisted of (1) a vertically mounted 3 mm diameter, 1.4 m high square capillary made of glass and (2) an image recording and analysis system. Gas and liquid were fed to the bottom of the capillary through a 3 mm diameter PVC tee-junction connection. Compressed air was fed through a pre-calibrated gas flowmeter to the tee-junction. Two manually operated control valves were used to regulate the gas flow rate. The first of these valves was placed between the compressed air flow line and the flow meter and was set to give a constant gauge pressure of 0.3 bar. The second valve, placed between the gas flowmeter and the tee was solely used in regulating the volumetric gas flow rate into the capillary. Demineralized water was fed from an elevated 10 L storage vessel into a pre-calibrated liquid flowmeter with the flow rate also adjusted by the use of a manually operated valve. Gravity provided the driving force for the flow of liquid from the storage vessel into the liquid flowmeter. This flow arrangement provided for an independent alteration of the gas and liquid flow rates. Liquid was discharged from the capillary into a 33 mm wide, 40 mm high disengagement zone at the top of the capillary. The image recording system consisted of a Photron Fastcam-ultima 40K high-speed video camera, a memory box and a CRT monitor display. Video movies captured by the high-speed camera were instantaneously stored in the memory box. The high-speed camera has the capability of capturing video movies at rates of between 25 and 4500 frames per second (fps). The CRT display showed in real time what was viewed through the high-speed camera. Data from the memory box were transferred to the PC for analysis.

3. Experimental procedure

Air was used as the gas phase and demineralized water as the liquid phase in all experiments carried out. Measurements were made of the gas holdup and volumetric mass transfer coefficient in each reactor configuration studied. Downcomer liquid velocity measurements were also made in the monolith and airlift loop reactors. At the start of each experimental run, the clear liquid height was set at 0.105 m in the gas–liquid separator of the short monolith loop reactor and 0.44 m in the gas–liquid separator of the tall monolith and airlift loop reactors. The clear liquid height in the bubble column was set at 1.6 m. The monolith and airlift loop reactors were operated in such a way that gas bubbles leaving the gas distributor traversed the riser and disengaged at the gas–liquid separator without entering the downcomer. This meant that the downcomer sections of these reactors were left free for liquid recirculation. Taylor bubble hydrodynamic experiments were carried out in the upflow single capillary.

3.1. Gas holdup measurements

Gas holdup measurements were made in the risers of the monolith and airlift loop reactors. In both the tall and short monolith loop reactors, the riser gas holdup was measured by trapping gas from the monolith channels into a measuring cylinder 6.3 cm in diameter and 1 m in height (see Fig. 3a). To achieve this, a hollow cylindrical metal rod with an inner diameter of 4 mm was fixed through a base plate consisting of a 9 mm-thick rubber pad glued underneath a 4 mm-thick plastic plate. The base plate had a diameter of 16 cm. The cylindrical metal rod was connected to the measuring cylin-

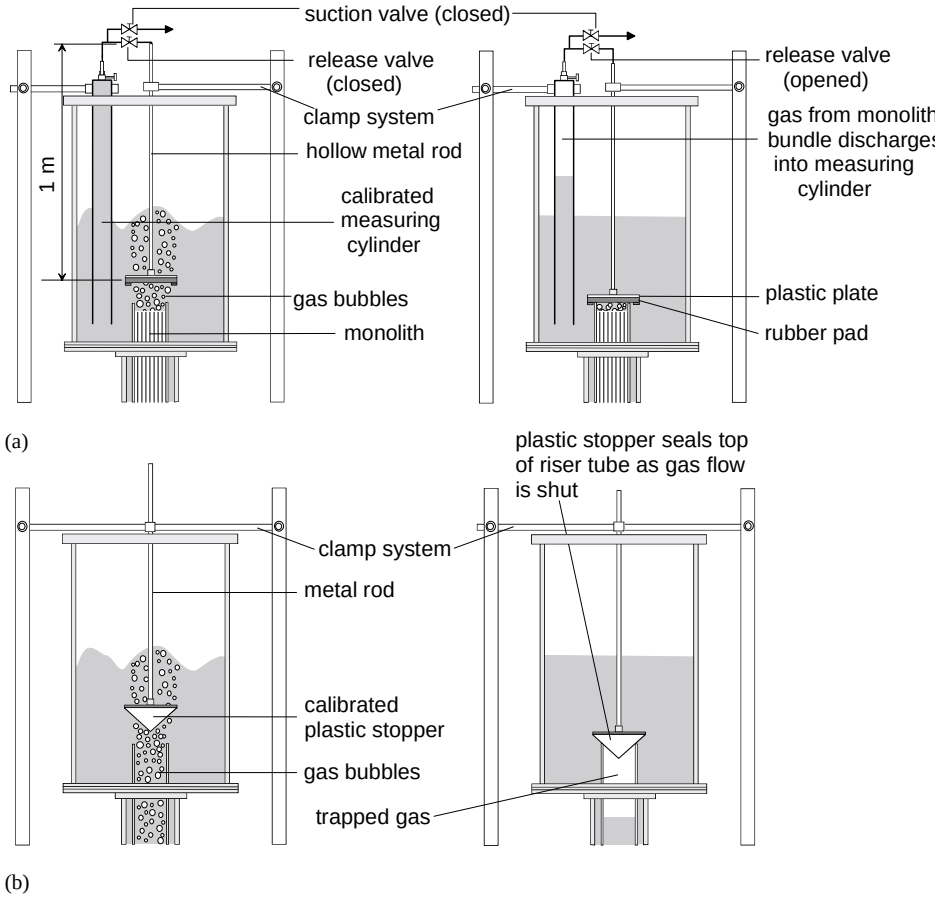

Fig. 3. Schematic representation of the procedures for determining the riser gas holdup in (a) the monolith loop reactors and (b) the airlift loop reactor. Further details are available elsewhere [20,21].

der via a manually operated 'release' valve. Before the start of each holdup experiment, the measuring cylinder was filled with demineralized water by opening the suction valve located at its top and activating a venturi jet pump to which this suction valve was connected. Both the measuring cylinder and hollow metal rod were vertically positioned in the gas–liquid separator using a system of clamps. The base plate of the hollow metal rod was also pre-positioned about 15 cm above the monolith riser tube. At the moment the gas flow into the column was shut, the hollow metal rod was instantaneously displaced so that the rubber pad on its base plate rested on the riser tube. In this way, gas bubbles were trapped in the monolith channels of the riser. By opening the release valve, the trapped bubbles were transferred to the measuring cylinder. Based on the volume of trapped gas, the riser gas holdup was determined. The holdup experiments were done in duplicate, and found to be consistent. Average values are reported.

The gas holdup in the riser section of the airlift loop reactor was measured by sealing the top of its riser column with a pre-calibrated plastic stopper at the moment gas flow into the column was shut down (see Fig. 3b). In this way, gas was trapped in the riser. The height of the trapped gas was read using a graduated rule affixed on the riser tube, from which the volume of gas and thus, the gas holdup were determined. For each gas flow rate in the airlift loop reactor, the gas holdup experiments were done twice with the mean holdup value presented.

Gas holdup values in the bubble column were obtained by a pressure difference method. For each gas flow rate, sufficient time was given for steady state to be reached after which the increase in liquid pressure at the higher of the two pressure taps used was recorded. This increase occurred due to the presence of gas bubbles in the column, causing the upward displacement of liquid. The measured pressure signals, obtained in the form of voltage readings were interpreted to obtain information on the gas holdups.

3.2. Downcomer liquid velocity measurements

Liquid velocity measurements were carried out in the downcomers of the monolith and airlift loop reactors. To do this, a pulse injection of a tracer was made just beneath the top of the downcomer, at a height of 0.54 m above the base of the short monolith reactor and 2.04 m above the base of the tall monolith and airlift reactors. Detection of the tracer was done using a conductivity probe placed at a height, $H_{\text{tracer}} = 0.46$ and 1.99 m below in the short monolith and

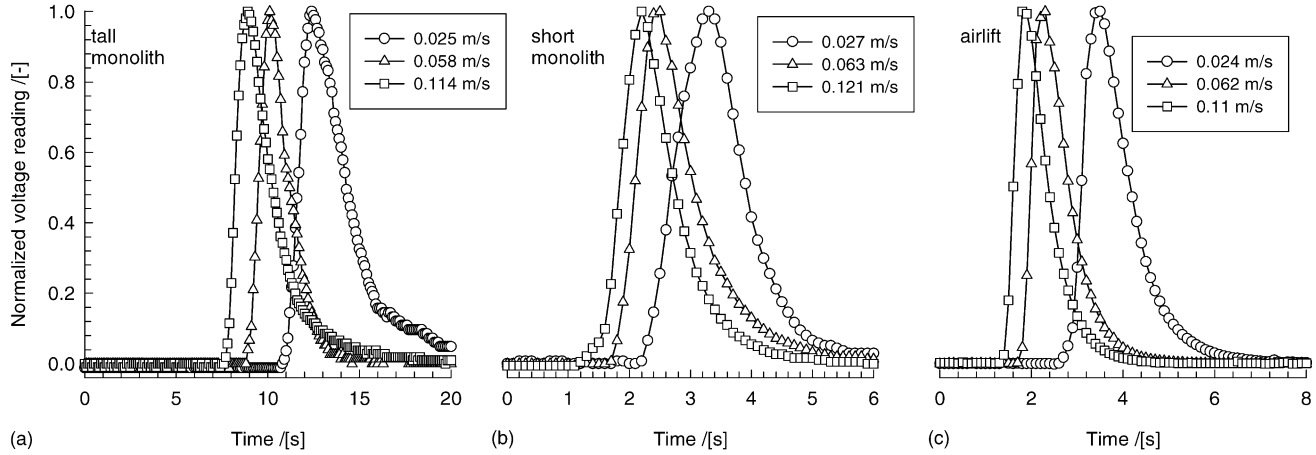

Fig. 4. Response data to tracer pulse input for the specified superficial gas velocities, U_G in the (a) tall monolith loop reactor, (b) short monolith loop reactor (c) airlift loop reactor.

tall monolith/airlift setups, respectively. The tracer used was saturated NaCl solution and between 0.3 and 0.5 mL was injected depending on the setup and experimental operating conditions. The conductivity probe used consisted of two copper wires, which were connected to a conductivity meter (Consort K920) and a PC. The tracer concentration detected by the conductivity probe was reflected as a voltage reading on the conductivity meter. Typical response curves are shown in Fig. 4a–c for the monolith and airlift loop reactors at three superficial gas velocities. Time zero on these plots corresponds to the exact moment at which tracer injection occurred. For a given superficial gas velocity, the liquid mean residence time, τ_L was obtained from the response curve using the relationship:

$$\tau_L = \frac{\int_0^\infty tV(t)\,dt}{\int_0^\infty V(t)\,dt} \quad (1)$$

where $V(t)$ is the voltage reading as a function of time. The mean liquid velocity in the downcomer U_{LD} was then calculated from:

$$U_{LD} = \frac{H_{tracer}}{\tau_L} \quad (2)$$

For each gas velocity, three liquid velocity measurements were carried out with the average U_{LD} values presented in this paper.

3.3. Volumetric mass transfer coefficient measurements

The volumetric mass transfer coefficient, k_La was determined by means of a dynamic oxygen absorption technique. An oxygen electrode (YSI Incorporated Model 5331) was used to measure the change in dissolved oxygen concentration. The electrode was inserted 0.27 m above the base of the short monolith loop reactor and 0.35 m above the base of the tall monolith and airlift loop reactors. It was inserted 0.05 m above the base of the bubble column. The actual measuring point in monolith and airlift loop reactors was in their downcomer sections (refer to Fig. 1). Readings given by the electrode were fed to a PC via an ammeter and an analogue-to-digital converter card. The change in dissolved oxygen concentration was reflected as a change in electrical current displayed on the ammeter. The electrode was made sensitive to the presence of dissolved oxygen by applying a 0.13 mg/L KCl solution between its tip and an outer membrane, made of Teflon. Dissolved oxygen was stripped from the liquid phase to a negligible concentration by the use of nitrogen sparged through the gas distributor. After the stripping operation, a step input of air was introduced into the reactor, with the uptake of oxygen into the liquid phase continuously monitored by the oxygen sensor. Sufficient time was given in each experimental run for the oxygen saturation concentration in the liquid, C_L^* to be reached. Data obtained were then interpreted to obtain volumetric mass transfer coefficient values by the use of reactor models developed.

Prior to conducting mass transfer experiments, the time constant of the oxygen sensor was determined by instantaneously inserting the oxygen electrode in a beaker of water that was saturated with oxygen by the continuous bubbling of air into it. Before this, the sensor was placed in a beaker of water from which oxygen had been completely stripped off with nitrogen and in which nitrogen was continuously bubbled. A typical experimental dynamic response for the oxygen sensor is shown in Fig. 5. The sensor constant, k_{sensor} was then determined by fitting the response to the relation:

$$\frac{C_{sensor}}{C_L^*} = 1 - e^{-k_{sensor}\,t} \quad (3)$$

For the example shown in Fig. 5, k_{sensor} was determined to be 0.5 s^{-1}. The membrane surrounding the oxygen electrode was replaced frequently and the sensor constant determined for each membrane. The value of k_{sensor} was found to vary in the range 0.4–0.51 s^{-1} for all experiments carried out.

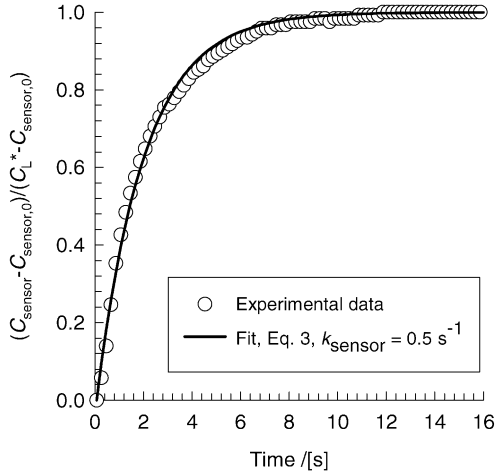

Fig. 5. Oxygen absorption dynamic response obtained from a water-filled glass beaker saturated with dissolved oxygen for determining the sensor constant.

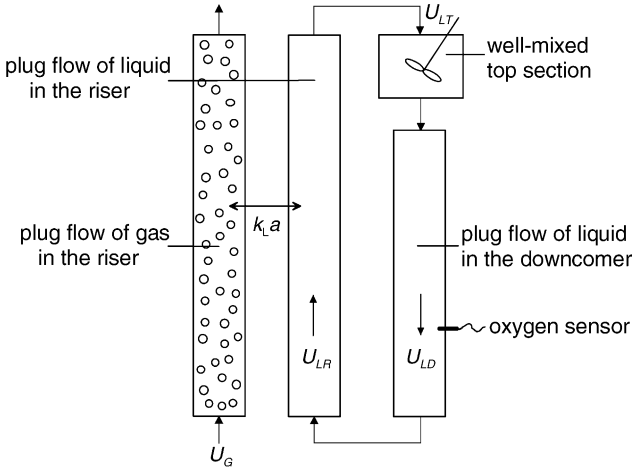

Fig. 6. Schematic representation of the reactor model used to determine k_La in the monolith and airlift loop reactors. Further details are available elsewhere [20,21].

3.4. Single capillary experiments

In determining the rise characteristics of Taylor bubbles in the square capillary, air and water flow rates were independently adjusted such that the superficial gas, U_G, and liquid, U_{LR}, velocities in the capillary corresponded to values obtained in the upflow monolith loop reactors previously discussed. The high-speed camera was positioned midway along the capillary height and adequately focused, enabling it to capture rising air bubbles and liquid slugs within a vertical window 0.2 m high. At that start of each experimental investigation, the gas and liquid control valves were regulated to obtain desired flow velocities. Once steady flow had been achieved, high-speed movies were made for a time span of 3 s at a capture rate of 2250 fps. By carrying out a frame-by-frame analysis of each movie, the bubble frequency, f_b, defined as the number of bubbles traversing the halfway point of the capillary per unit time, was determined. The bubble rise velocity, V_b was also determined from the movie analysis by registering the time required for a gas bubble to rise 0.2 m along the capillary height. For each gas and liquid flow rate, the V_b reported is the average obtained from five randomly selected bubbles. The mean unit cell length, L_{UC} for each U_G and U_L combination was obtained from:

$$L_{UC} = \frac{V_b}{f_b} \tag{4}$$

4. Models for determining k_La

4.1. Monolith and airlift loop reactors

A common reactor model was developed for the monolith and airlift loop reactors for obtaining volumetric mass transfer coefficient values from experimental dynamic oxygen absorption curves based on the following assumptions:

- Plug flow of gas and liquid in the riser section of the reactor. For the monolith reactors, tall and short, the minimum number of units cells is 11 and this rises to values in excess of 50. Therefore the assumption of plug flow is justified.
- Plug flow of liquid in the downcomer section.
- A well-mixed gas–liquid separator section.

The riser section of the reactor is assumed to extend to the dispersion height. This means that gas bubbles in the gas–liquid separator constitute a part of the riser, i.e. no gas bubbles are assumed to be present in the gas–liquid separator. The gas free gas–liquid separator is referred to as the top section in the model developed. A diagram of the model is shown in Fig. 6. The governing mass balance equations for this model are:

Plug flow of gas in the riser:

$$\varepsilon_G \frac{\partial C_G}{\partial t} = -U_G \frac{\partial C_G}{\partial h} - k_L a \left(\frac{C_G}{m} - C_{LR} \right) \tag{5}$$

Plug flow of liquid in the riser:

$$\varepsilon_L \frac{\partial C_{LR}}{\partial t} = -U_{LR} \frac{\partial C_{LR}}{\partial h} + k_L a \left(\frac{C_G}{m} - C_{LR} \right) \tag{6}$$

Well-mixed gas–liquid separator section at the top:

$$\frac{\partial C_{LT}}{\partial t} = -U_{LT} \frac{\Delta(C_{LT})}{H_T} \tag{7}$$

Plug flow of liquid in the downcomer:

$$\frac{\partial C_{LD}}{\partial t} = U_{LD} \frac{\partial C_{LD}}{\partial h} \tag{8}$$

Sensor correction equation:

$$\frac{dC_{sensor}}{dt} = k_{sensor}(C_{LD} - C_{sensor}) \tag{9}$$

ε_G and ε_L are the gas and liquid holdups in the riser section of the monolith and airlift loop reactors. k_La is the volumetric mass transfer coefficient per unit volume of dispersion

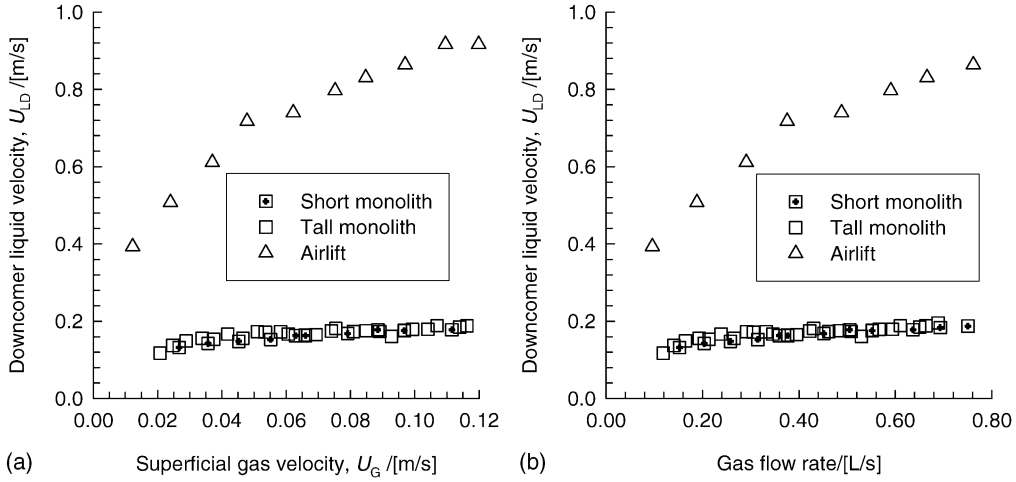

Fig. 7. Variation in measured downcomer liquid velocity, U_{LD} with superficial gas velocity, U_G for tall and short monolith reactors and the airlift reactor.

(gas + liquid) in the riser section of the monolith and airlift loop reactors. U_G is the superficial gas velocity with respect to the riser section of the reactor (based on open area available for flow of gas and liquid phases in case of monolith configurations) while U_{LR}, U_{LT} and U_{LD} are the superficial liquid velocities in the riser, top section and downcomer, respectively. The values of U_{LD} as determined experimentally were used in the reactor model. Fig. 7a and b show the experimentally determined U_{LD} values as a function of U_G and gas flow rate for the monolith and airlift reactors respectively. For a given U_G, U_{LD} is the same for both the short and tall monolith loop reactors, signifying similar hydrodynamic behaviour in both reactors. Once U_{LD} is known the U_{LR} and U_{LT} values are determined from geometry considerations, using the known cross-sectional areas. H_T is the dispersion height of the top section and m, the solubility coefficient of oxygen in water; $m = 28$. Eqs. (5)–(9) are subject to the following boundary conditions:

- At time $t = 0$, $C_G = C_{G,inlet}$
- At time $t = 0$, $C_{LR} = C_{LD} = 0$
- $C_{LR,in} = C_{LD,out}$
- $C_{LD,in} = C_{LT,out}$
- $C_{LT,in} = C_{LR,out}$

Solving the Eqs. (5)–(9) involved discretizing their spatial derivates. A first-order backward difference approximation was used. The Method of Lines solution procedure was adopted with 50 grid points used to represent the total dispersion height in the reactor. A FORTRAN program was written to handle this, utilizing the ODE solver LSODE [24] in double precision. Fig. 8a and b show sample k_La fits in the tall and short monolith loop reactors for $U_G = 0.061$ and 0.142 m/s respectively. The k_La values obtained from these fits are 0.137 and 0.2 s^{-1}, respectively. Also shown in Fig. 8a and b with dashed line are the dynamic uptake curves if the liquid leaving at the top of the monolith section were to be saturated with dissolved oxygen. The maximum possible saturation rate was determined assuming perfect mixing of the liquid in the gas–liquid separator and downcomer. The data in Fig. 8a for operation of the tall monolith reactor at $U_G = 0.061$ m/s shows that the measured dynamic uptake curve is quite close to the saturation values. For the tall monolith reactor operating at superficial gas velocities $U_G > 0.07$ m/s the dynamic uptake curve was close to, or indistinguishable from, the saturation curve. Therefore the fitted k_La values for $U_G > 0.07$ m/s are all considered to be suspect. In contrast, all experimental dynamic oxygen absorption curves over the entire range of operating conditions obtained in the short monolith reactor were well below saturation values. This is illustrated by the dynamic oxygen uptake curve shown in Fig. 8b for operation of the short monolith reactor at $U_G = 0.142$ m/s, the highest gas velocity used in this campaign. Even for this case the measured uptake dynamics lies well below the anticipated uptake curve were the liquid leaving at the top to be saturated, shown by the dashed line. The fitted k_La values for the short monolith reactor are therefore trustworthy for the entire range of U_G values. The above discussions underline the need for extreme caution in interpreting the oxygen uptake dynamics to obtain k_La in monolith loop systems.

Fig. 8c shows a sample fit in the airlift loop reactor. In this case, $U_G = 0.087$ m/s and $k_La = 0.103\ s^{-1}$.

4.2. Bubble column reactor

In interpreting experimental dynamic oxygen absorption curves to obtain k_La values in the bubble column, a model was developed based on the gas phase being in plug flow and a well-mixed liquid phase. The resulting oxygen mass balance equations are:

$$\varepsilon_G \frac{\partial C_G}{\partial t} = -U_G \frac{\partial C_G}{\partial h} - k_La\left(\frac{C_G}{m} - C_L\right) \quad (10)$$

$$\varepsilon_L \frac{dC_L}{dt} = \frac{k_La}{H}\int_0^H \left(\frac{C_G}{m} - C_L\right) dh \quad (11)$$

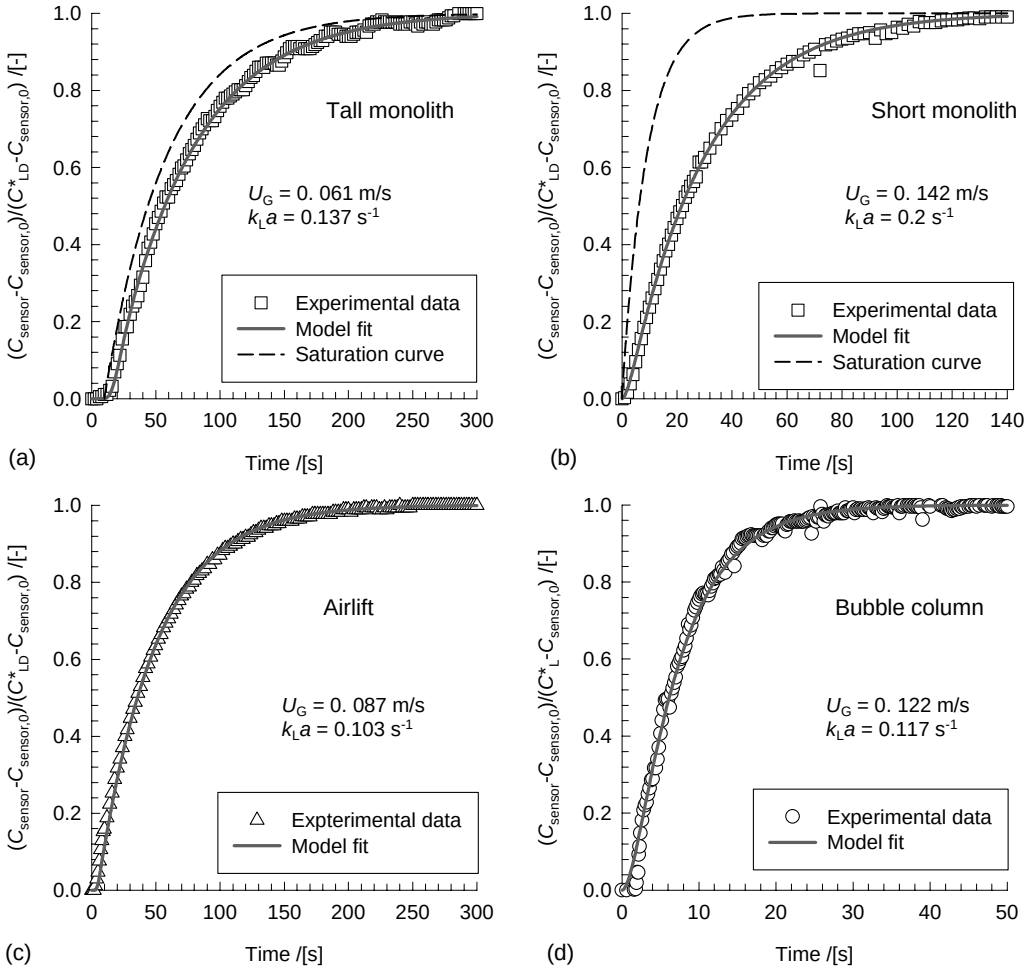

Fig. 8. Oxygen absorption dynamics for the specified superficial gas velocities, U_G in the (a) tall monolith loop reactor, (b) short monolith loop reactor, (c) internal airlift loop reactor, (d) bubble column, as well as the reactor model fits obtained for each case in obtaining k_La values.

$$\varepsilon_L \frac{dC_{sensor}}{dt} = k_{sensor}(C_L - C_{sensor}) \quad (12)$$

ε_G and ε_L are the gas and liquid holdups in the bubble column. k_La is the volumetric mass transfer coefficient per unit volume of dispersion in the bubble column while H is the dispersion height. Eqs. (10)–(12) were also solved using the Method of Lines with the following boundary conditions: at time $t = 0$, $C_G = C_{G,inlet}$, and $C_L = 0$. A typical bubble column model fit for obtaining the value of k_La is shown

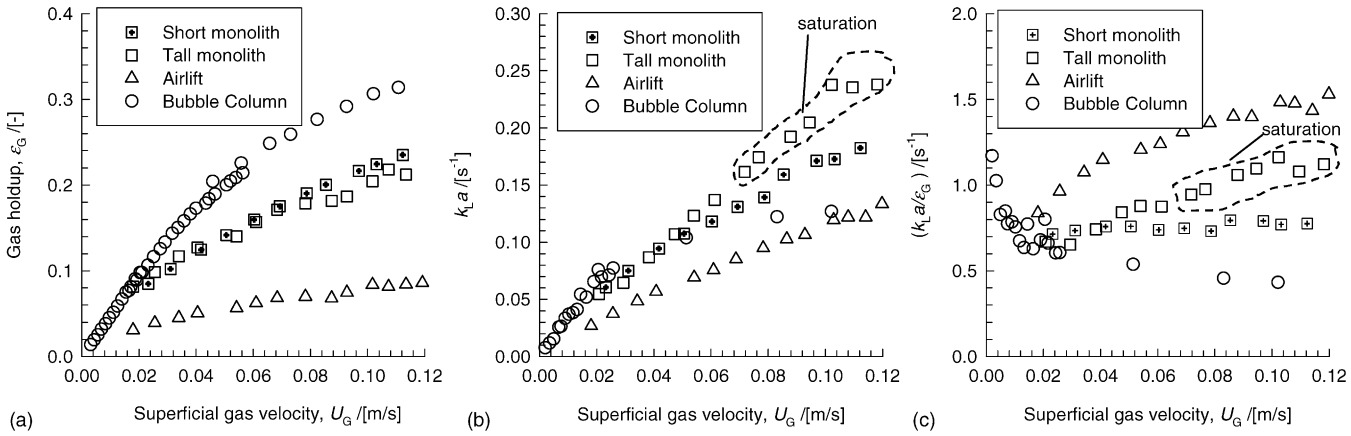

Fig. 9. Variation of superficial gas velocity, U_G with (a) gas holdup, ε_G, (b) volumetric mass transfer coefficient, k_La and (c) k_La/ε_G in each of the reactor configurations investigated.

in Fig. 8d. For this case, $U_G = 0.122$ m/s and the k_La value obtained is $0.117\,s^{-1}$.

5. Results and discussions

The measured data on the gas holdup, ε_G, volumetric mass transfer coefficient, k_La, and the ratio k_La/ε_G, as a function of the superficial gas velocity U_G based on the open area available for flow of the phases, for the reactor configurations investigated are summarized in Fig. 9a–c. The gas holdup in the airlift reactor is the lowest of the reactor configurations investigated. This is because of the high liquid circulation velocities in the airlift column (see Fig. 7); these high circulation velocities result in a very low slip velocity between the gas and liquid phases in the riser, resulting in a lower gas holdup. The very low slip between the gas and liquid phases also results in a very uniform distribution of gas bubbles, with very little coalescence. It is also remarkable to note that the gas holdup in the tall and short monolith loop reactors are virtually identical. This is an important conclusion from a scale up view point.

The monolith reactors show significantly higher values of k_La than conventionally used bubble columns and internal airlift reactor configurations, when the comparison is made at the same U_G. As discussed earlier, the k_La values for the tall monolith reactor operating at $U_G > 0.07$ m/s are not trustworthy due to the possibility of reaching oxygen saturation at the top. Therefore the doubtful values are encircled with the dashed region marked "saturation". For $U_G < 0.07$ m/s, there is very good agreement in k_La values for tall and short monoliths.

We note that the mass transfer coefficient per unit volume of dispersed gas bubbles, k_La/ε_G, is higher for monoliths than for a conventional bubble column, emphasising the superiority of monoliths for carrying out fast reactions. k_La/ε_G is also independent of U_G in the short monolith reactor taking on a constant value of about 0.76. Interestingly, k_La/ε_G for the airlift column is higher than that of the monolith, this is due to the fact that the gas holdup in the airlift is considerably lower than in the monolith reactor; at such low gas holdups the bubbles are uniform and small in size and the bubbles travel upward with very little backmixing of the gas or liquid phases.

In the monoliths, we have Taylor flow inside the capillaries [2,4], resulting in trains of bubbles that are separated from one other by liquid slugs [25]; see Fig. 10a. The bubbles are surrounded by a thin liquid film, that is of the order of 50–200 μm, depending on the gas and liquid superficial velocities, U_G and U_{LR} through each monolith channel [18]. Fig. 10b and c show the single capillary data (denoted by circles) on L_{UC} and V_b obtained from the experiments. The corresponding information obtained by observing the rise of Taylor bubbles through a small crack, 0.13 m high, in one of the outer channels of the tall monolith loop reactor and recording it with the high-speed video camera at 750 fps is also shown (square symbols). Sample high-speed video recordings of the Taylor bubbles rising in the outer channel can be viewed on our website [20]. In the single capillary measurements, for fixed values of U_G and U_{LR} there is practically no variation in the values of L_{UC} and V_b. This is in sharp contrast with the information obtained from the video recordings of the outer channel. There is a very wide spread in the L_{UC} values, as evidenced by the error bars indicating the standard deviation of measurements (about 30–50 unit cells were analysed for each $U_G + U_{LR}$). The mean value of L_{UC} agrees reasonably well with those from single capillary measurements. The wide variation of the unit cell lengths in the monolith has implications for mass transfer from Taylor bubbles.

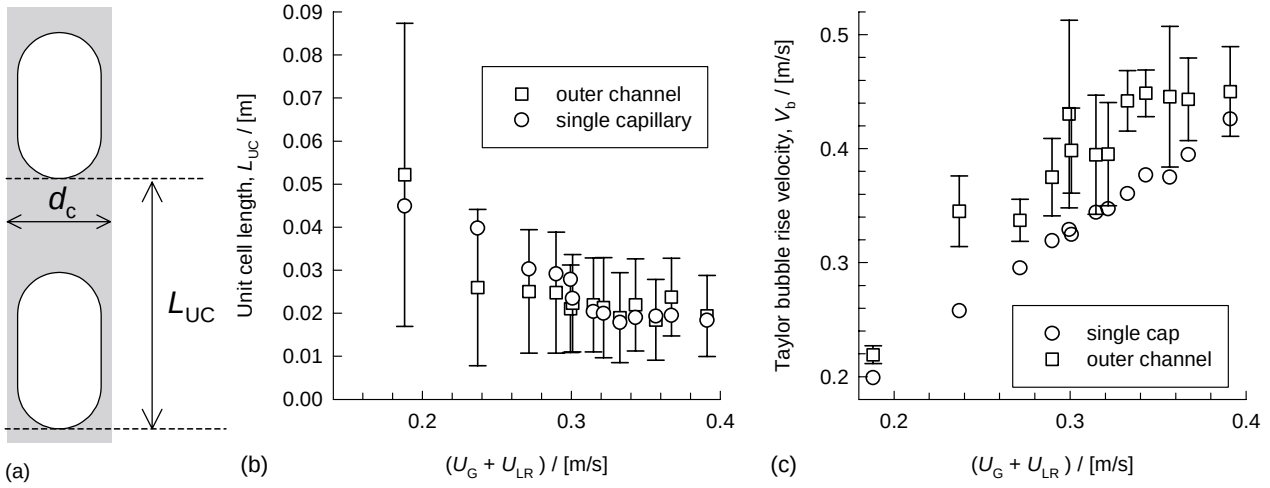

Fig. 10. (a) Schematic of a unit cell for Taylor flow in a single capillary. (b) Influence of ($U_G + U_{LR}$) on the unit cell length. (c) The Taylor bubble rise velocity as a function of ($U_G + U_{LR}$). The round symbols in (b) and (c) refer to data obtained from single capillary experiments. The square symbols refer to the measurements on the outer channel of the tall monolith. The error bars represent the standard deviations obtained from frame-by-frame analysis of the video recordings.

From Fig. 10c we note that the Taylor bubble rise velocity V_b as measured in the single capillary are lower than the corresponding values in the outer channel. Also shown by the continuous solid line is the parity line with ($U_G + U_{LR}$). The larger difference between V_b and ($U_G + U_{LR}$) would suggest increased downflow in the monolith as compared to the single capillary. A possible reason is non-uniform distribution of gas and liquid phases through the channels of the monolith. Using magnetic resonance imaging (MRI), Mantle et al. [26] showed that a wide range of bubble sizes exist in a 400 cpsi downflow monolith. They also concluded that bubble velocity is not stable with time. These two phenomena have also been observed in the outer channel of the 35 cpsi upflow monolith reactor studied.

Recently, van Baten and Krishna have developed a fundamental model for calculation of the volumetric mass transfer coefficient for Taylor bubbles rising in circular capillaries [27]. Their model recognises two contributions to mass transfer: (1) from the two hemispherical caps at either end, and (2) from the film surrounding the bubble:

$$k_L a = k_{L,cap} a_{cap} + k_{L,film} a_{film} \quad (13)$$

with

$$k_{L,cap} = 2\sqrt{\frac{2\mathcal{D}V_b}{\pi^2 d_c}} \quad (14)$$

and

$$k_{L,film} \approx 2\sqrt{\frac{\mathcal{D}}{\pi t_{film}}} \quad (15)$$

where t_{film}, the contact time of the liquid film with the rising Taylor gas bubble, can be estimated as $t_{film} = L_{UC}\varepsilon_G / V_b$. The calculations of the film, cap and total (=film + cap) $k_L a$ values using Eqs. (13)–(15), using the V_b, ε_G and L_{UC} data obtained from the outer channel of the monolith, are shown in Fig. 11. The experimental $k_L a$ values agree very well with the film contribution, $k_{L,film} a_{film}$, which is the major contributor to the mass transfer process [27]. It is likely that the cap contribution predicted by the model is too optimistic due to the fact that the front and rear ends of the Taylor bubbles are more flattened. This would lead to a lower surface area than afforded by the two hemispherical caps assumed in the model. It appears that the volumetric mass transfer coefficients can be estimated from information on the Taylor bubble hydrodynamics.

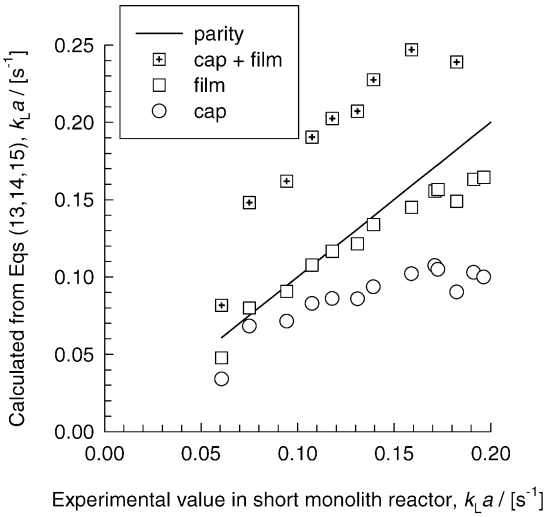

Fig. 11. Comparison of experimentally determined volumetric mass transfer coefficients $k_L a$, obtained in the short monolith loop reactor with the predictions using Eqs. (13)–(15). The hydrodynamic data on V_b, ε_G and L_{UC} were those obtained from the outer channel of the monolith. The continuous solid line represents the parity plot.

6. Conclusions

The hydrodynamics and mass transfer characteristics of monolith loop reactors, with upflow of gas and liquid phases through the channels, have been investigated in this study and compared with conventional internal airlift reactor and bubble column configurations. The following major conclusions can be drawn from this work.

(1) The volumetric mass transfer coefficient, $k_L a$, is significantly higher for monolith reactors than for airlift and bubble columns. This improvement is due to the superior mass transfer characteristics of Taylor flow in narrow capillaries.
(2) The superior mass transfer of monolith reactors provides interesting opportunities for application to three-phase reaction systems for process intensification.
(3) The volumetric mass transfer coefficient in monolith reactors can be estimated from information on Taylor bubble hydrodynamics, in particular values of V_b, ε_G and L_{UC}.
(4) Our experiments in the tall monolith also highlight that extreme care should be taken in interpreting the dynamic oxygen uptake curves for tall monoliths in view of the anticipated problem of the liquid reaching saturation conditions.

Acknowledgements

Corning GmbH is gratefully acknowledged for provision of the cordierite square-channel monolith. We also acknowledge useful discussions with Dr. T. Boger of Corning. The Netherlands Foundation for Scientific Research—Chemical Sciences Division (NWO—CW), provides a research program subsidy. Sasol Technology Netherlands BV is gratefully acknowledged for partial financial support. We also thank a referee of this paper for pointing out the danger of saturation occurring in the tall monolith reactor.

Appendix A. Nomenclature

a	gas–liquid interfacial area per unit volume of dispersion; except for bubble columns the dispersion within the riser section is considered ($m^2\,m^{-3}$)
C_G	gas phase oxygen concentration (mol/m^3)
C_L	liquid phase oxygen concentration (mol/m^3) or arbitrary units
C_{LD}	liquid phase oxygen concentration in the downcomer (mol/m^3) or arbitrary units
C_{LR}	liquid phase oxygen concentration in the riser (mol/m^3)
C_{sensor}	liquid phase oxygen concentration indicated by the sensor, arbitrary units
C_{LT}	liquid phase oxygen concentration in the gas–liquid separator (top section) (mol/m^3)
d_c	capillary channel dimension (m)
$\mathcal{D}$	liquid phase diffusivity (m^2/s)
f_b	Taylor bubble frequency in single capillary (s^{-1})
H	total dispersion height (m)
H_T	dispersion height in the gas–liquid separator (top section) (m)
H_{tracer}	distance travelled by tracer in downcomer liquid velocity experiments (m)
k_L	liquid-side mass transfer coefficient (m/s)
k_{sensor}	sensor time constant (s^{-1})
L_{UC}	unit cell length (m)
m	solubility coefficient of oxygen in water, dimensionless
t_{film}	contact time of liquid film with Taylor gas bubble (m/s)
U_G	superficial gas velocity in the riser (m/s)
U_{LD}	downcomer superficial liquid velocity (m/s)
U_{LR}	riser superficial liquid velocity (m/s)
U_{LT}	top section superficial liquid velocity (m/s)
V	voltage reading on conductivity meter (mV)
V_b	Taylor bubble rise velocity (m/s)

Greek letters

ε_G	gas holdup in the riser, dimensionless
ε_L	liquid holdup in the riser, dimensionless
τ_L	liquid mean residence time in the downcomer (s)

Subscripts and superscripts

cap	refers to hemispherical cap
film	refers to liquid film
in	refers to conditions into a given section of the reactor
inlet	refers to conditions at the inlet of the reactor
out	refers to conditions *out* of a given section of the reactor
0	initial condition
$*$	refers to saturation concentration

References

[1] S. Irandoust, B. Andersson, Monolithic catalysts for nonautomobile applications, Catal. Rev., Sci. Eng. 30 (1988) 341–392.

[2] T. Boger, S. Roy, A.K. Heibel, O. Borchers, A monolith loop reactor as an attractive alternative to slurry reactors, Catal. Today 79 (2003) 441–451.

[3] L.L. Crynes, R.L. Cerro, M.A. Abraham, Monolith froth reactor—development of a novel 3-phase catalytic-system, A. I. Ch. E. J. 41 (1995) 337–345.

[4] F. Kapteijn, T.A. Nijhuis, J.J. Heiszwolf, J.A. Moulijn, New non-traditional multiphase catalytic reactors based on monolithic structures, Catal. Today 66 (2001) 133–144.

[5] R.K. Edvinsson, A. Cybulski, A comparison between the monolithic reactor and the trickle-bed reactor for liquid-phase hydrogenations, Catal. Today 24 (1995) 173–179.

[6] R.K. Edvinsson, A.M. Holmgren, S. Irandoust, Liquid-phase hydrogenation of acetylene in a monolithic catalyst reactor, Ind. Eng. Chem. Res. 34 (1995) 94–100.

[7] T.A. Nijhuis, F.M. Dautzenberg, J.A. Moulijn, Modeling of monolithic and trickle-bed reactors for the hydrogenation of styrene, Chem. Eng. Sci. 58 (2003) 1113–1124.

[8] S. Irandoust, O. Gahne, Competitive hydrodesulfurization and hydrogenation in a monolithic reactor, A. I. Ch. E. J. 36 (1990) 746–752.

[9] A.A. Klinghoffer, R.L. Cerro, M.A. Abraham, Influence of flow properties on the performance of the monolith froth reactor for catalytic wet oxidation of acetic acid, Ind. Eng. Chem. Res. 37 (1998) 1203–1210.

[10] X.C. Quan, H.C. Shi, Y.M. Zhang, J.L. Wang, Y. Qian, Biodegradation of 2,4-dichlorophenol in an air-lift honeycomb-like ceramic reactor, Process Biochem. 38 (2003) 1545–1551.

[11] R.M. de Deugd, F. Kapteijn, J.A. Moulijn, Using monolithic catalysts for highly selective Fischer–Tropsch synthesis, Catal. Today 79 (2003) 495–501.

[12] R.M. de Deugd, R.B. Chougule, M.T. Kreutzer, F.M. Meeuse, J. Grievink, F. Kapteijn, J.A. Moulijn, Is a monolithic loop reactor a viable option for Fischer–Tropsch synthesis? Chem. Eng. Sci. 58 (2003) 583–591.

[13] T.A. Nijhuis, M.T. Kreutzer, A.C.J. Romijn, F. Kapteijn, J.A. Moulijn, Monolithic catalysts as more efficient three-phase reactors, Catal. Today 66 (2001) 157–165.

[14] A. Stankiewicz, Process intensification in in-line monolithic reactor, Chem. Eng. Sci. 56 (2001) 359–364.

[15] J.J. Heiszwolf, L.B. Engelvaart, M.G. van den Eijnden, M.T. Kreutzer, F. Kapteijn, J.A. Moulijn, Hydrodynamic aspects of the monolith loop reactor, Chem. Eng. Sci. 56 (2001) 805–812.

[16] J.J. Heiszwolf, M.T. Kreutzer, M.G. van den Eijnden, F. Kapteijn, J.A. Moulijn, Gas-liquid mass transfer of aqueous Taylor flow in monoliths, Catal. Today 69 (2001) 51–55.

[17] M.T. Kreutzer, P. Du, J.J. Heiszwolf, F. Kapteijn, J.A. Moulijn, Mass transfer characteristics of three-phase monolith reactors, Chem. Eng. Sci. 56 (2001) 6015–6023.

[18] M.T. Kreutzer, Hydrodynamics of Taylor Flow in Capillaries and Monolith Reactors, Ph.D. Thesis, Delft University of Technology, Delft, The Netherlands, 2003.

[19] T.A. Nijhuis, M.T. Kreutzer, A.C.J. Romijn, F. Kapteijn, J.A. Moulijn, Monolithic catalysts as efficient three-phase reactors, Chem. Eng. Sci. 56 (2001) 823–829.

[20] C.O. Vandu, J. Ellenberger, R. Krishna, Hydrodynamics and Mass Transfer in an Upflow Monolith Loop Reactor, http://ct-cr4.chem.uva.nl/Monolith/, 2003.

[21] C.O. Vandu, J. Ellenberger, R. Krishna, Hydrodynamics and Mass Transfer in an Internal Airlift Reactor, http://ct-cr4.chem.uva.nl/AirliftExpt/, 2003.

[22] C.O. Vandu, R. Krishna, Slurry Bubble Column Research, http://ct-cr4.chem.uva.nl/BubbleColumnExpt/, 2003.
[23] C.O. Vandu, J. Ellenberger, R. Krishna, Taylor Bubble Rise in Circular and Square Capillaries, University of Amsterdam, Amsterdam, The Netherlands, http://ct-cr4.chem.uva.nl/SingleCapillary/, 2004.
[24] A.C. Hindmarsh, Livermore Solver for Ordinary Differential Equations, Lawrence Livermore National Laboratory, Livermore, California, http://www.llnl.gov/CASC/, 2001.
[25] T.C. Thulasidas, M.A. Abraham, R.L. Cerro, Bubble-train flow in capillaries of circular and square cross-section, Chem. Eng. Sci. 50 (1995) 183–199.
[26] M.D. Mantle, A.J. Sederman, L.F. Gladden, S. Raymahasay, J.M. Winterbottom, E.H. Stitt, Dynamic MRI visualization of two-phase flow in a ceramic monolith, A. I. Ch. E. J. 48 (2002) 909–912.
[27] J.M. van Baten, R. Krishna, CFD simulations of mass transfer from Taylor bubbles rising in circular capillaries, Chem. Eng. Sci. 59 (2004) 2535–2545.